Insights from Selective Non-phosphinic Inhibitors of MMP-12 Tailored to Fit with an S$_1$′ Loop Canonical Conformation*[S]

Laurent Devel[‡], **Sandra Garcia**[‡], **Bertrand Czarny**[‡], **Fabrice Beau**[‡], **Evelyne Lajeunesse**[‡], **Laura Vera**[‡], **Dimitris Georgiadis**[§], **Enrico Stura**[‡], and **Vincent Dive**[‡1]

From the [‡]Commissariat à l'Energie Atomique, Service d'Ingénierie Moléculaire de Protéines, CE-Saclay, 91191 Gif/Yvette Cedex, France and the [§]Laboratory of Organic Chemistry, Department of Organic Chemistry, University of Athens, Panepistimiopolis, Zografou, 15771 Athens, Greece

After the disappointment of clinical trials with early broad spectrum synthetic inhibitors of matrix metalloproteinases (MMPs), the field is now resurging with a new focus on the development of selective inhibitors that fully discriminate between different members of the MMP family with several therapeutic applications in perspective. Here, we report a novel class of highly selective MMP-12 inhibitors, without a phosphinic zinc-binding group, designed to plunge deeper into the S$_1$′ cavity of the enzyme. The best inhibitor from this series, identified through a systematic chemical exploration, displays nanomolar potency toward MMP-12 and selectivity factors that range between 2 and 4 orders of magnitude toward a large set of MMPs. Comparison of the high resolution x-ray structures of MMP-12 in free state or bound to this new MMP-12 selective inhibitor reveals that this compound fits deeply within the S$_1$′ specificity cavity, maximizing surface/volume ratios, without perturbing the S$_1$′ loop conformation. This is in contrast with highly selective MMP-13 inhibitors that were shown to select a particular S$_1$′ loop conformation. The search for such compounds that fit precisely to preponderant S$_1$′ loop conformation of a particular MMP may prove to be an alternative effective strategy for developing selective inhibitors of MMPs.

The association of matrix metalloproteinases (MMPs)[2] with a variety of pathological states has stimulated impressive efforts over the past 20 years to develop synthetic compounds able to block efficiently (1–7) and selectively the uncontrolled activity of these enzymes (8). Extremely potent inhibitors of MMPs have been developed, but in most cases these compounds act as broad spectrum inhibitors of MMPs (9). The arguments that have been proposed to explain the difficulties in identifying inhibitors able to differentiate one MMP from another include: (a) marked sequence similarities between the catalytic domains of MMPs, (b) a well conserved enzyme active site topology (backbone RMSD between the MMP catalytic domains is 0.7–0.8 Å), and (c) the mobility of residues in the so-called S$_1$′ specificity loop (10, 11).

MMPs form a group of 23 proteins in humans, all of which contain a catalytic domain belonging to the zinc metalloproteinase family (12, 13). Retrospective analysis suggests that the incorporation of strong zinc-binding groups, such as hydroxamate functions, potentiates MMP inhibition but unfortunately in an indiscriminate manner affecting most members of the MMP family (7), as well as other unrelated zinc-proteinases (14). The use of a less avid zinc-binding group, like the phosphoryl group present in phosphinic peptide transition state analogs, has led to a second generation of more selective MMP inhibitors, like the selective inhibitors reported for MMP-12 (macrophage-metalloelastase) (15). The third generation MMP inhibitors possess no zinc-binding group and exploit mainly the depth of the S$_1$′ cavity present in most MMPs (16, 17). This strategy has led to the discovery of the first extremely selective MMP-13 inhibitors, such as compound **1** (Scheme 1). The x-ray structure of MMP-13 in complex with compound **1** confirms that this compound enters deeply into the S$_1$′ cavity of MMP-13 and involves an unusual S$_1$′ loop conformation characterized by the presence of an additional S$_1$′ side pocket, a feature absent from other MMP-13·inhibitor complex x-ray structures. Part of the S$_1$′ side pocket of MMP-13 involves residues of the so-called S$_1$′ loop, whose size and sequence varies among MMPs. The selectivity of compound **1** toward MMP-13 has been explained by the presence of Gly[248], a unique feature of the S$_1$′ loop of MMP-13 that allows it to adopt a main chain conformation that is energetically disfavored for other MMPs (16). Another selective inhibitor without zinc-binding group has also been recently reported (compound **2**; Scheme 1) for the MMP-8, MMP-13 pair (18). Interestingly, the x-ray structure of **2** bound to MMP-8 again reveals the presence of an S$_1$′ side pocket, with the distal part of **2** protruding into this pocket, in a manner similar to that observed in the MMP-13·**1** complex. This suggests that the presence of an S$_1$′ side pocket is not restricted to MMP-13 and might also occur in other MMPs through a displacement of the S$_1$′ loop relative to the protein body. To explore this possibility, a series of compounds with no phosphinic zinc-binding group have been developed and screened against various MMPs, with the objective to identify highly selective MMP-12 inhibitors. Such attempts previously achieved only the identification of compounds with low

---

[1] To whom correspondence should be addressed: CEA, Service d'Ingénierie Moléculaire de Protéines (SIMOPRO), 152, CE-Saclay, 91191 Gif/Yvette Cedex, France. Tel.: 33-1- 69083585; Fax: 33-1-69089071; E-mail: vincent. dive@cea.fr.

[2] The abbreviations used are: MMP, matrix metalloproteinase; ACE, angiotensin-converting enzyme; NEP, neprilysin; AHA, acetohydroxamic acid; RMSD, root mean square deviation.
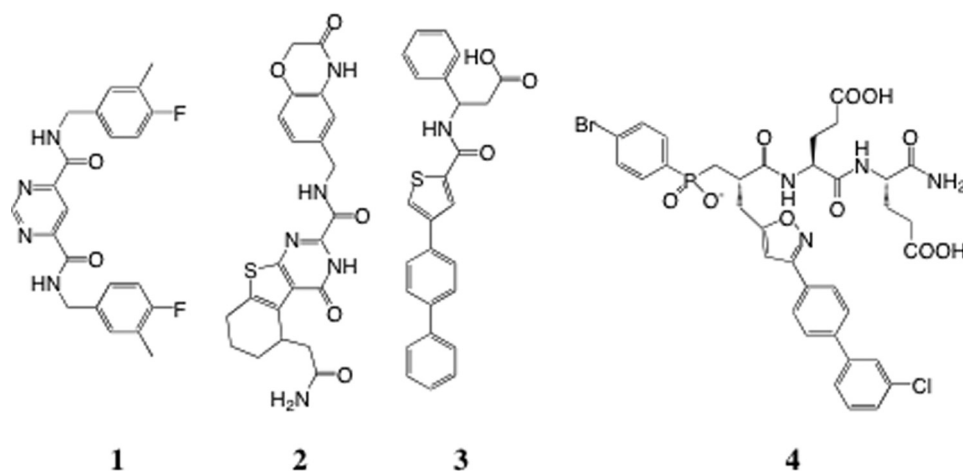
SCHEME 1. **Chemical structures of compounds 1–4.**

potency toward MMP-12 and poor selectivity profile (like **3** in Scheme 1) (19).

The drive toward the development of highly selective MMP-12 inhibitors is justified by recent studies showing the overexpression of MMP-12 in several human pathologies, such as emphysema (20), osteoarthritis (21), atherosclerosis (22), aneurisms (23), giant cell arteritis (24), and chronic obstructive pulmonary disease (25). Recently, based on a large clinical study, testing for an association between both asthma and chronic obstructive pulmonary disease and single-nucleotide polymorphisms in the gene encoding MMP-12, a detrimental role was attributed to the overexpression of MMP-12 (26). In animal models, mice deficient in MMP-12 were shown to be less susceptible to emphysema (27–29), atherosclerosis (30), and aneurisms (21). Furthermore, the need for MMP inhibitors with better selectivity profile is also justified by the poor outcomes observed in preclinical studies using broad spectrum inhibitors (31, 32) and the opposing roles that MMPs play in pathologies like cancer (33) and atherosclerosis progression (30). These studies have clearly indicated the absolute need to specifically target the MMPs involved in pathology progression and not those counteracting it. Ultimately, highly selective inhibitors are essential tools to obtain proof of principle for the efficacy of a chemical intervention in animal models, as compared with gene invalidation.

EXPERIMENTAL PROCEDURES

Chemical Synthesis—Malonic building blocks as precursors of pseudo-peptides **5–36** were first synthesized in solution and then assembled to peptide sequence on solid support. After cleavage, the resulting pseudo-peptides **5–36** were purified by preparative reverse phase HPLC, and their purity was assessed by analytical HPLC and high resolution mass spectrometry analysis. On the basis of this criteria, all of the compounds possess purity at >95%. For further details on synthesis, see supplemental "Experimental Procedures" and the analytical data of each synthesized compound (supplemental Table S2).

Enzyme Assays—All of the inhibition assays were carried out in 50 mM Tris-HCl buffer, pH 6.8, 10 mM CaCl$_2$ at 25 °C as described previously (15, 34). ACE inhibition assays were per-

formed using Mca-Ala-Ser-Asp-Lys-Dpa-OH as substrate (15 mM) and human somatic ACE (0.5 nM) from R & D Systems. NEP inhibition assays were performed using Mca-Arg-Pro-Pro-Gly-Phe-Ser-Pro-Dpa-OH from Enzo Life Sciences, as substrate (5 mM, K_m = 2 mM) and human NEP (0.5 nM) from R & D Systems. MMPs inhibition assays were performed using Mca-Pro-Leu-Gly-Leu-Dpa-Ala-Arg-NH$_2$, as substrate (13 mM, K_m = 8.5 mM) and human MMPs (nanomolar range concentration) from R & D Systems (15), except for human MMP-12 that was produced and purified as described previously (35). The substrate and enzyme concentrations for the experiments were chosen so as to remain well below 10% of substrate utilization and to observe the initial rates. For each inhibitor, the percentage of inhibition was determined in triplicate experiments at five inhibitor concentrations, chosen to observe a 20–80% range of inhibition. K_i values were determined using the method proposed by Horovitz and Leviski (36) (supplemental Table S3). Continuous assays were performed by recording the fluorescence increase induced by the cleavage of fluorogenic substrates, using black, flat-bottomed, 96-well nonbinding surface plates (Corning-Costar, Schiphol-Rijk, The Netherlands). Fluorescence signals were monitored using a Fluoroscan *Ascent* photon counter spectrophotometer (Thermo-Labsystems, Courtaboeuf, France) equipped with a temperature control device and a plate shaker.

Crystallization—The protein inhibitor solution for crystallization consisted of 0.53 mM of the catalytic domain of the F67D mutant of human MMP12 residues 106–263 with 100 mM acetohydroxamic acid (AHA) to prevent self-degradation of the proteinase prior to crystallization in 3 mM CaCl$_2$, 200 mM NaCl with 20 mM Tris-HCl at pH 7.5 and 10 mM of one of the four selective inhibitors (compounds **5**, **9**, **14**, and **36** lyophilized). This solution was mixed in a ratio 1:1 with reservoir solution containing the precipitant to give drops of 2 μl (initial volume). Initial crystallization tests made use of previously published conditions and of *ab initio* screening with the "Stura" screens (37) (MD1–20 from Molecular Dimensions; condition 12; three-dimensional: 22.5% PEG 10,000, 200 mM imidazole malate, pH 8.5). The drops were equilibrated by sitting drop vapor diffusion for 1–4 days at 20 °C in a cooled incubator before streak seeding (38). Optimization for each inhibitor consisted of small variations in the PEG concentration and in some cases changes in ionic strength, buffer (Tris-HCl, imidazole, cacodylate, glycine) or in the molecular weight of polyethylene glycol (supplemental Table 1S). For data collection, the crystals were transferred to a cryo-protecting solution consisting of 27% PEG 8000, 15% monomethyl-PEG 550, 10% glycerol, 90 mM Tris-HCl, pH 8.0, then picked up with a loop, and cryo-cooled in liquid nitrogen.
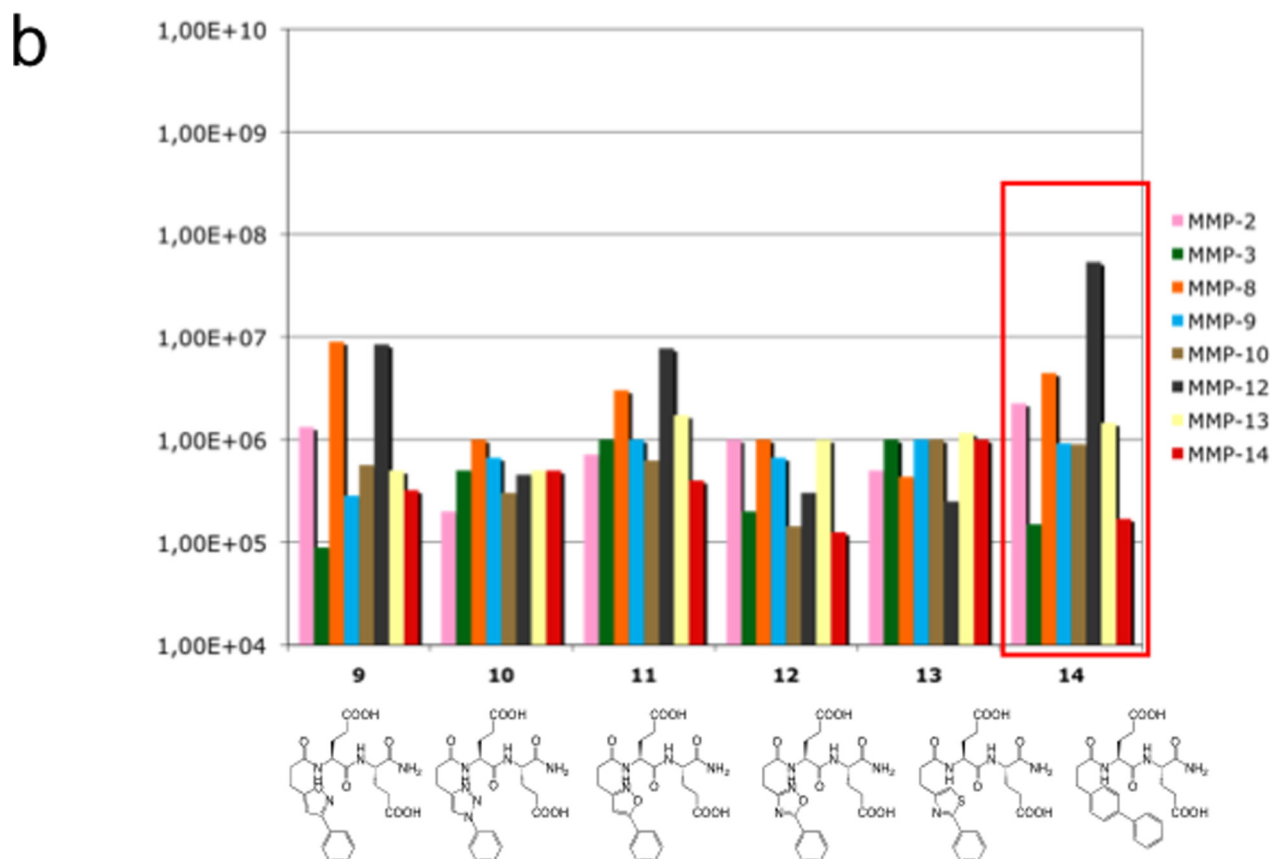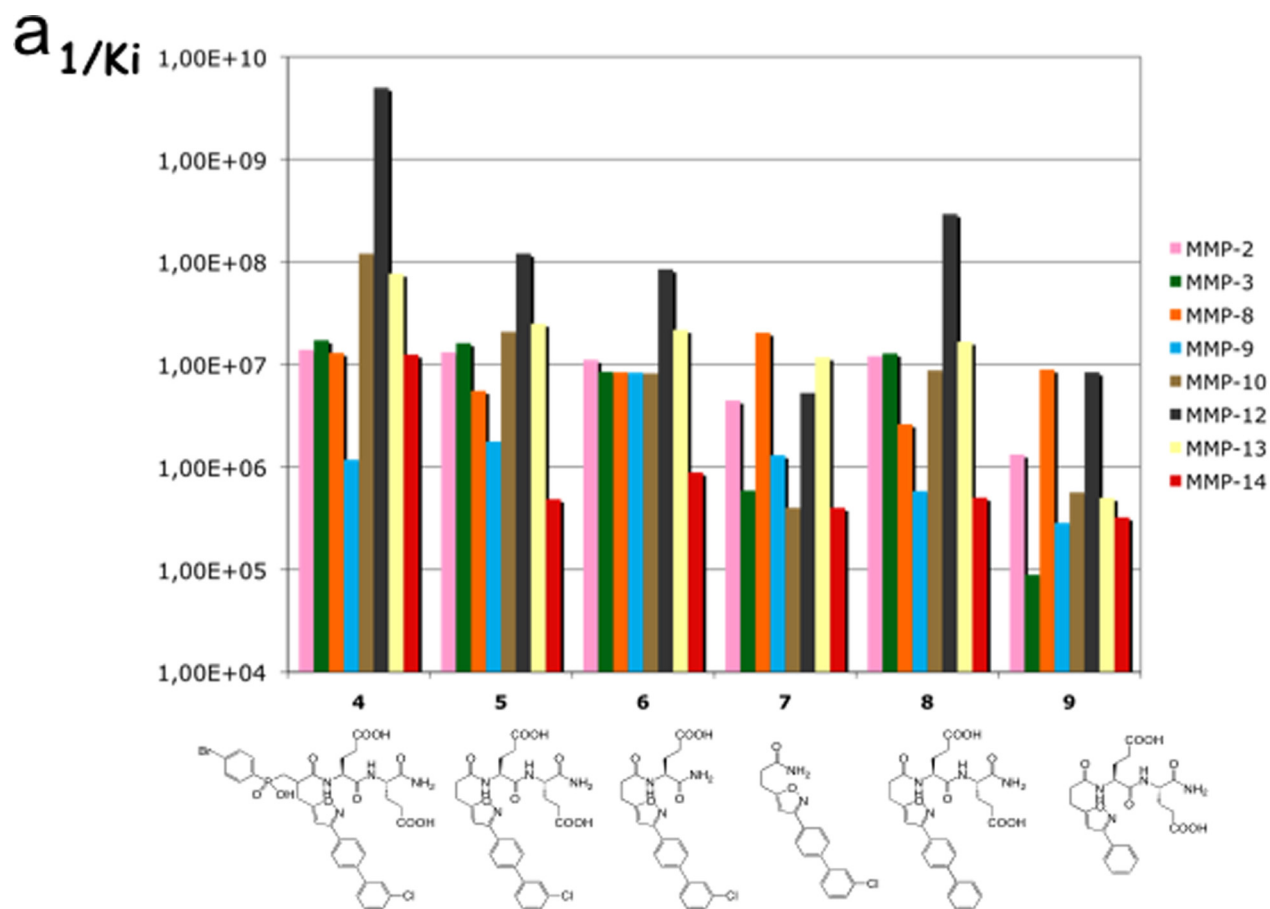
FIGURE 1. *a*, effects of the RXP470 deconstruction; *b*, the nature of proximal ring on the MMP selectivity profile. For each MMP, the $1/K_i$ values are reported.
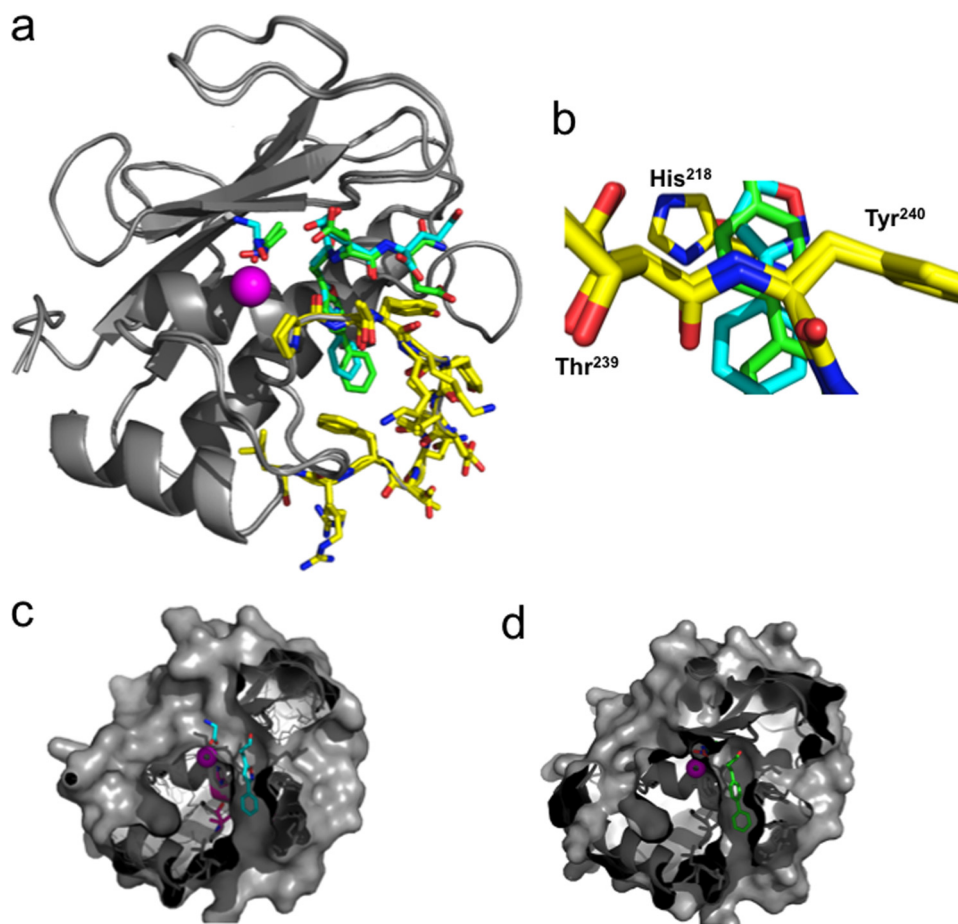
FIGURE 2. *a*, overlay of MMP-12 complexes with compounds **9** and **14**. MMP-12 is shown in ribbon representation (*gray*) with the active site zinc in *purple*. Compounds **9** and **14** and AHA are shown as sticks with nitrogen (*blue*) and oxygen (*red*), and carbon atoms are colored according to the compound (**9**, *cyan*; **14**, *green*). S_1' loop residues are highlighted as sticks with carbon atoms in *yellow*. *b*, detailed view at the S_1' cavity entrance, showing the respective positioning of inhibitor side chain in respect to His[218] and the peptide bond located between Thr[239] and Tyr[240]. Cross-section of MMP-12 molecular surface with compound **9** (*c*) and **14** (*d*) showing the positioning of the inhibitor side chain into the S_1' cavity.

Data Structure Determination and Refinement—The data for the MMP-12-inhibitor complexes were collected at the European Synchrotron Radiation Facility, beam lines ID14-2 and ID23-1 (Grenoble, France) or at the Soleil Synchrotron Facility (St. Aubin, France) at 100 K from single crystals. Crystals diffracted to high resolution (1.9–1.3 Å). Data reduction was carried out with MOSFLM (39). The crystals belong to the tetragonal space group $P2_12_12$ with one molecule in the asymmetric unit with cell parameters similar to Protein Data Bank entry 1RMZ (11). This entry with the inhibitor removed was used for molecular replacement carried out with MOLREP (40). Subsequently structure solutions have been carried out by rigid body refinement with REFMAC (41), in all cases where lattice parameters have not varied substantially. The constraint files for the inhibitor have been generated with Monomer Library Sketcher from the CCP4 suite of programs (42). The refined ligand was then fitted in the difference electron density maps (omit σA-weighted $F_o - F_c$) calculated and displayed using XFIT from the XtalView suite of programs (43). In all cases a single conformation was seen for the inhibitor except for compound **5** where the chloride atom can be found in two distinct positions. The second position refined with occupancy below

0.2 was omitted from the final deposited file. Final fitting and stereochemical analysis of the refined model was carried out with COOT (44). The figures were made with PyMOL from DeLano Scientific (45).

Protein Data Bank Accession Number—The coordinates and structure factors for the catalytic subunit of human MMP12-inhibitor complexes have been deposited in the RCSB Protein Data Bank with the following codes: compound **5**, code 3LIL; compound **9**, code 3LIR; compound **14**, code 3LJG; and compound **36**, code 3LIK (supplemental Table S1).

Molecular Modeling—The molecular models of the interaction of compound **36** with MMPs was achieved with program CHARMM (version 27), using version 22. The initial position of compound **36** in MMP active sites was obtained by superimposition of the main chain atoms of the MMP-12·**36** complex crystal structure onto that of other crystal structures of MMPs (Protein Data Bank code for MMP-2 (code 1QIB), MMP-3 (code 1G49), MMP-8 (code 1I76), MMP-9 (code 2OVZ), and MMP-13 (code 3I7G), respectively. The geometrical and nonbonded parameters for compound **36** were derived from *ab initio* quantum calculations with the program GAUSSIAN98. These calculations were done at the MP2 level of theory using a 6–31+G(d,p) basis set. The starting complex structures were then refined by energy minimization and molecular dynamics with CHARMM (15).

RESULTS

From Phosphinic Inhibitors to Non-zinc Binding Inhibitors— We previously reported compound **4** (RXP470; Scheme 1) as a potent and selective inhibitor of MMP-12, in which the isoxazole side chain in conjunction with the Glu-Glu motif was shown to play a key role in the selectivity of the inhibitor (15). In **4**, the phosphoryl group (PO_2^-) is thought to interact with the zinc ion of the MMP-12 active site, as previously observed in the x-ray structure of complexes between phosphinic peptide inhibitors and other MMP members (46, 47). Starting from compound **4**, a series of new compounds was generated by removal of the phosphinic moiety (Fig. 1*a*) as in compound **5**, resulting in a concomitant loss in potency and selectivity. Similar trends were observed when either the Glu-Glu motif (compounds **6** and **7**) or the isoxazole side chain (compounds **8** and **9**) were modified. These first results led us to evaluate the role
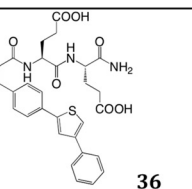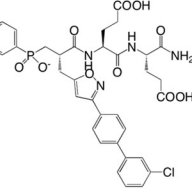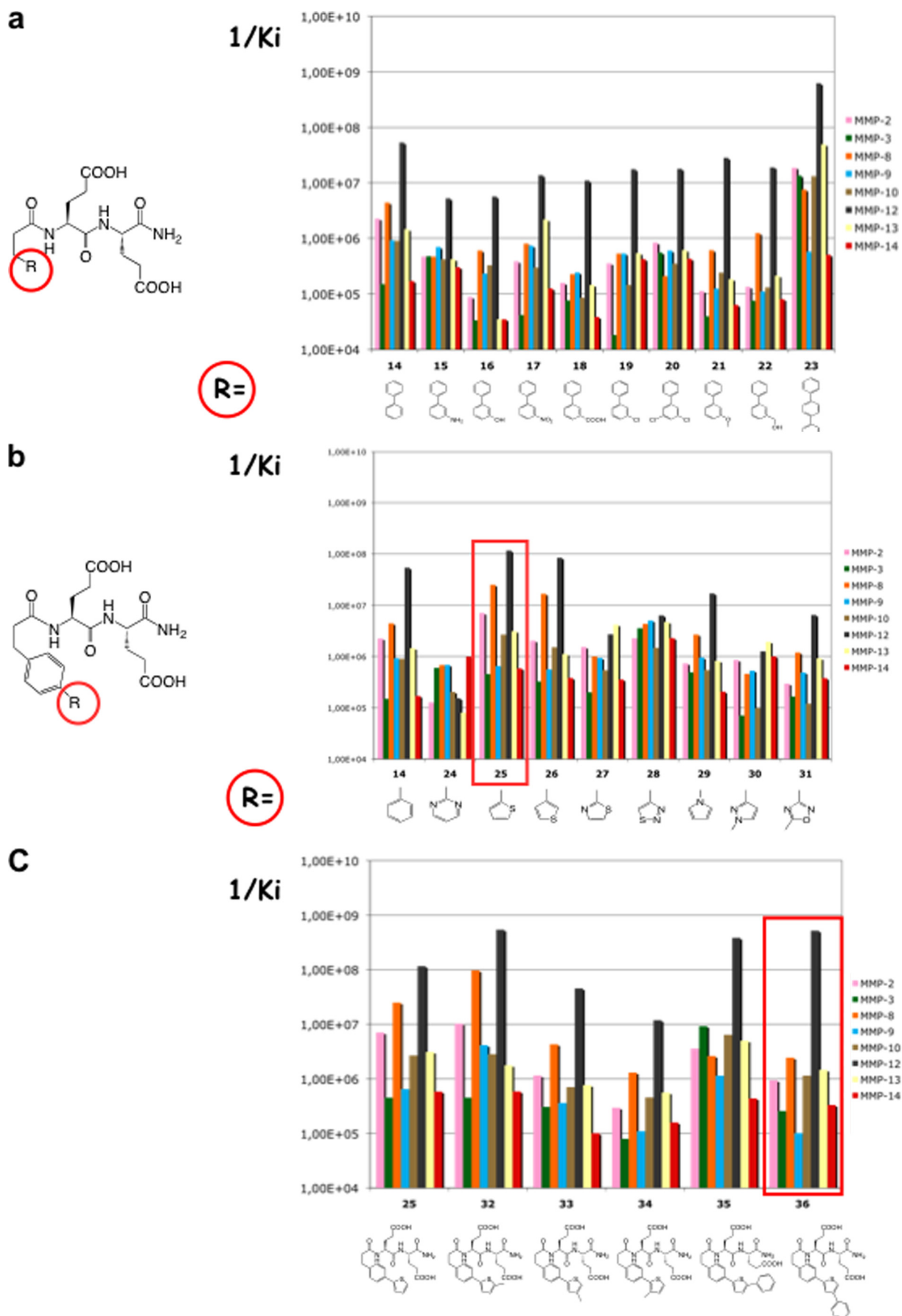
FIGURE 3. *a*, effects of the distal phenyl modification. *b*, nature of distal ring. *c*, thiophene modification on the MMP selectivity profile.

TABLE 1

Comparison of compounds 36 and 4 potency towards MMPs and their selectivity factors towards MMP-12

K_i values were determined in 50 mM Tris/HCl buffer, pH 6.8, 10 mM $CaCl_2$ at 25 °C.

Compounds		MMP-1h	MMP-2h	MMP-3h	MMP-7h	MMP-8h	MMP-9h	MMP-10h	MMP-12h	MMP-13h	MMP-14h	TACE	ACE	NEP
36	Ki (nM)	>10000	1060	3880	2010	410	>10000	872	1,92	684	3010	>10000	>10000	>10000
	Selectivity factor	>5200	550	2020	1047	213	>5200	454	1	356	1568	>5200	>5200	>5200
4	Ki (nM)	>10000	192	40	626	271	850	8,3	0.19	49	140	>10000	>10000	>10000
	Selectivity factor	>52000	>1000	210	>3200	>1400	>5200	43	1	257	736	>52000	>52000	>52000

of the isoxazole ring trough its substitution by other five-member rings (compounds **10**–**13**). As shown in Fig. 1*b*, with the exception of compound **11**, a loss of potency was observed highlighting the role played by hetero-atoms in these five-member rings. However, moving to a six-member phenyl ring resulted in compound **14** with a better selectivity profile in favor of MMP-12.

From Isoxazole to Phenyl Ring in the P$_1$′ Position—To gain some insights on the molecular factors contributing to the change in selectivity profile between compounds **9** and **14**, x-ray structures of their corresponding complexes with the MMP-12 catalytic domain were determined at high resolution, 1.9 and 1.31 Å, respectively (supplemental Table S1 and text). In these structures (Fig. 2*a*), the zinc atom is chelated respectively by a glycine (compound **9**) or an acetohydroxamic acid (AHA) molecule (compound **14**) (the presence of these small zinc-binding molecules originates from the co-crystallization buffer in the case of glycine or the addition of AHA to prevent MMP-12 autolysis, see "Experimental Procedures"). Overall, these structures confirm that the P$_1$′, P$_2$′, and P$_3$′ side chains in these inhibitors point toward their corresponding enzyme subsites (S$_1$′, S$_2$′, and S$_3$′), with no direct interaction between the zinc ion and inhibitor atoms. This observation is sustained by the lack of electron density between glycine or AHA and compounds **9** and **14**, as well as the distances between the P$_1$′ Cα inhibitor atoms and the zinc ion (4.4 and 4.5 Å, respectively). Residues of the S$_1$′ loop in both structures adopted almost similar orientations (Fig. 2*a*, *yellow stick*). However, because of the change in ring size, in **14** the P$_1$′ side chain enters more deeply into the S$_1$′ cavity, compared with **9** (Fig. 2, *b–d*). As a result of the phenyl shift, a better stacking is achieved between the first phenyl moiety of inhibitor **14** and His[218] side chain on one side and on the other side with the peptide bond located between Thr[239] and Tyr[240] (Fig. 2*b*). As expected, the S$_1$′ cavity in these structures appears to be partially empty, suggesting that the bottom part of the S$_1$′ cavity could be further probed by adding groups to the para or meta position on the second phenyl group in **14** (Fig. 2*d*).

Based on the above considerations, another set of compounds was designed by introducing various small substituents on the distal phenyl group of compound **14**. This series did not lead to major improvements in inhibitory potency (Fig. 3*a*). Some compounds (compounds **18** and **21**) displayed an improved selectivity profile, but their potency toward MMP-12 remained too low (K_i = ~100 nM). Further elongation of the P$_1$′ side chain by adding a third phenyl strongly increased the inhibitor potency (compound **23**) but at the expense of inhibitor selectivity. These results led us to explore alternative cycles in the distal part of the P$_1$′ side chain (Fig. 3*b*). With the exception of a thiophene ring (compounds **25** and **26**), most compounds in this series exhibited lower potency compared with **14**.

For chemistry considerations, compound **25** was selected for further modification (Fig. 3*c*). The introduction of a methyl at the α position relative to the sulfur atom in the thiophene ring led to marked changes both in potency and selectivity toward MMP-12 (compound **32**). In contrast, the same modification at β or γ position of the thiophene sulfur atom decreased potency (compounds **33** and **34**). With a phenyl, the β substitution (compound **36**) provided better results than the α one in terms of selectivity (compound **35**) (the γ position was discarded in this case to avoid steric clash within the S$_1$′ cavity). As compared with our starting compound (compound **4**, RXP470), compound **36** is slightly less potent toward MMP-12 and displays overall a similar selectivity profile toward a set of nine MMPs (Table 1), except for MMP-3 and MMP-10, where **36** is 10-fold less potent as compared with **4**. No inhibition of TACE (TNF-α-converting enzyme), ACE, and NEP was observed when **36** was tested up to a 10 mM concentration.

Crystal Structure of Compound 36 Bound to MMP-12—A high resolution x-ray structure of MMP-12 in complex with inhibitor **36** was solved in the presence of AHA (1.8 Å). In this complex, **36** adopts a very well defined structure (Fig. 4, *a* and *b*), with improved complementary fit between the P$_1$′ side chain of the inhibitor and the S$_1$′ cavity. Compounds **14** and **36** possess in common the Glu-Glu motif and the first phenyl ring.
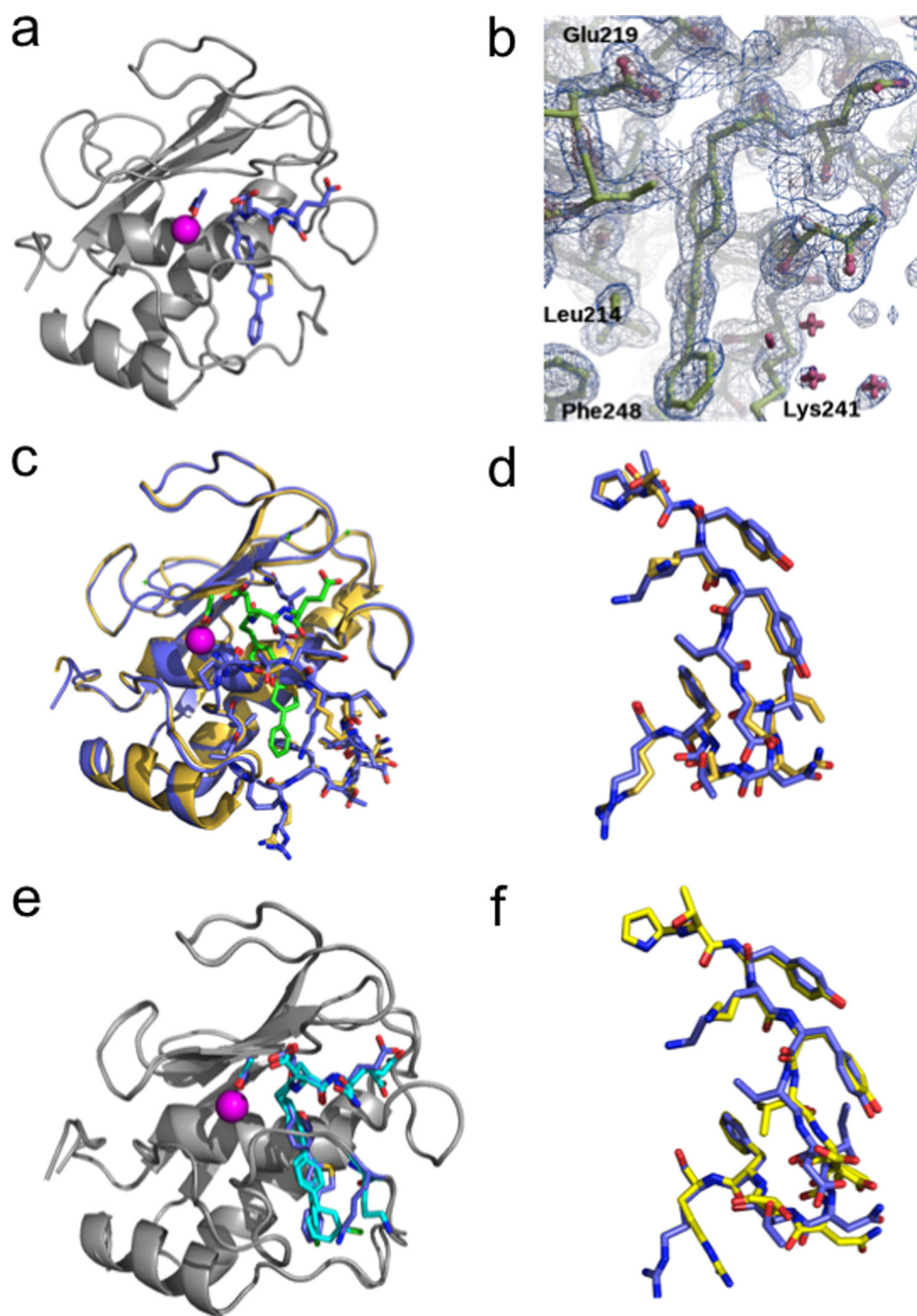
FIGURE 4. *a*, complex of MMP-12 with compound **36** in presence of AHA. Carbon atoms of 36 and AHA are shown as sticks colored *light blue*. *b*, $2F_{obs} - F_{calc}$ electron density map (1σ, *blue*; 4σ, *brown*) of the inhibitor binding region. *c*, overlay between complexes of MMP-12 with AHA (*beige*) or with **36** in presence of AHA (*blue*). AHA and **36** are shown as stick models with their carbon atoms in *green*. The S_1' loop of each complex is emphasized in sticks for each complex: AHA/MMP12 (*beige*; Protein Data Bank code 1Y93) and **36**·MMP-12 in presence of AHA (*blue*). The RMSD on Cα for this superposition is 0.43 Å. *d*, a close-up view of S_1' loop (residues 236–249) as in *c* (RMSD for this segment: 0.31 Å on Cα; 1.03Å for all atoms). *e*, overlay between complexes of MMP-12 with **5** (*cyan*) or with **36** (*blue*) in presence of AHA. The RMSD on Cα for the superposition is 0.35Å. *f*, a close-up view of the S_1' loop in complexes between MMP-12 and **5** (*yellow stick*) or with **36** (*blue stick*). The RMSD for the superposition of residues 236–249 is 0.61 Å on Cα and 1.44 Å for all atoms).

residues (Val[235], Tyr[240], Lys[241], Val[243], and Phe[248]) (Fig. 5*a*). This optimal accommodation relies on the bent structure of the inhibitor P_1' side chain induced by the thiophene ring. The above observations led us to wonder whether the inhibitor P_1' side chain position in the S_1' cavity might induce the concomitant conformational shift of the S_1' loop. To address this issue, we compared the crystal structures of MMP-12 in complex with **36** in the presence of AHA and MMP-12 complexed to AHA (Protein Data Bank code 1Y93, 1.03 Å) (11). The two MMP-12 structures overlay with only minor differences in their S_1' loop conformations, with the exception of Lys[241] side chain (Fig. 4, *c* and *d*; RMSD in figure legend). In presence of **36**, the Lys[241] side chain appears to fold back over the distal phenyl of **36** (Figs. 4*c* and 5*a*), with the ϵ CH$_2$ of Lys[241] making a CH-π interaction with the phenyl ring of the inhibitor, whereas in the MMP-12·AHA complex, the lysine side chain points toward the solvent (Fig. 4*c*). Overall, this comparison supports the view that the accommodation of the **36** P_1' side chain into the S_1' cavity can be realized without major rearrangement of the MMP-12 S_1' loop canonical conformation.

Compound 5 versus 36—Compounds **5** and **36** incorporate P_1' side chains of similar size but display markedly different selectivity profiles. To gain some insights into the molecular determinants that may explain this difference, x-ray structures of **5** in complex with MMP-12 were also solved in the presence of AHA (1.8 Å). Overall, in these two MMP-12 crystal structures, the protein adopts almost the same structure (Fig. 4, *e* and *f*), but on closer inspection the differences are observed between the S_1' loop residue conformation (Fig. 4*f*) and in the packing of the P_1' side chains

Comparison of their x-ray structures in interaction with MMP-12 revealed that these parts shared by the two inhibitors adopt almost the same binding mode. However, **36** achieves a larger number of Van der Waal's contacts between the distal part of the inhibitor (thiophene-phenyl) and several MMP-12

of compounds **5** and **36** and residues within the MMP-12 S_1' cavity (Fig. 5, *a* and *b*). In the MMP12·**5** complex, the distal chloro-phenyl group points toward Lys[241], pushing the lysine side chain toward the solvent (Fig. 5*b*). In contrast, in the MMP12·**36** complex, the distal phenyl points in the
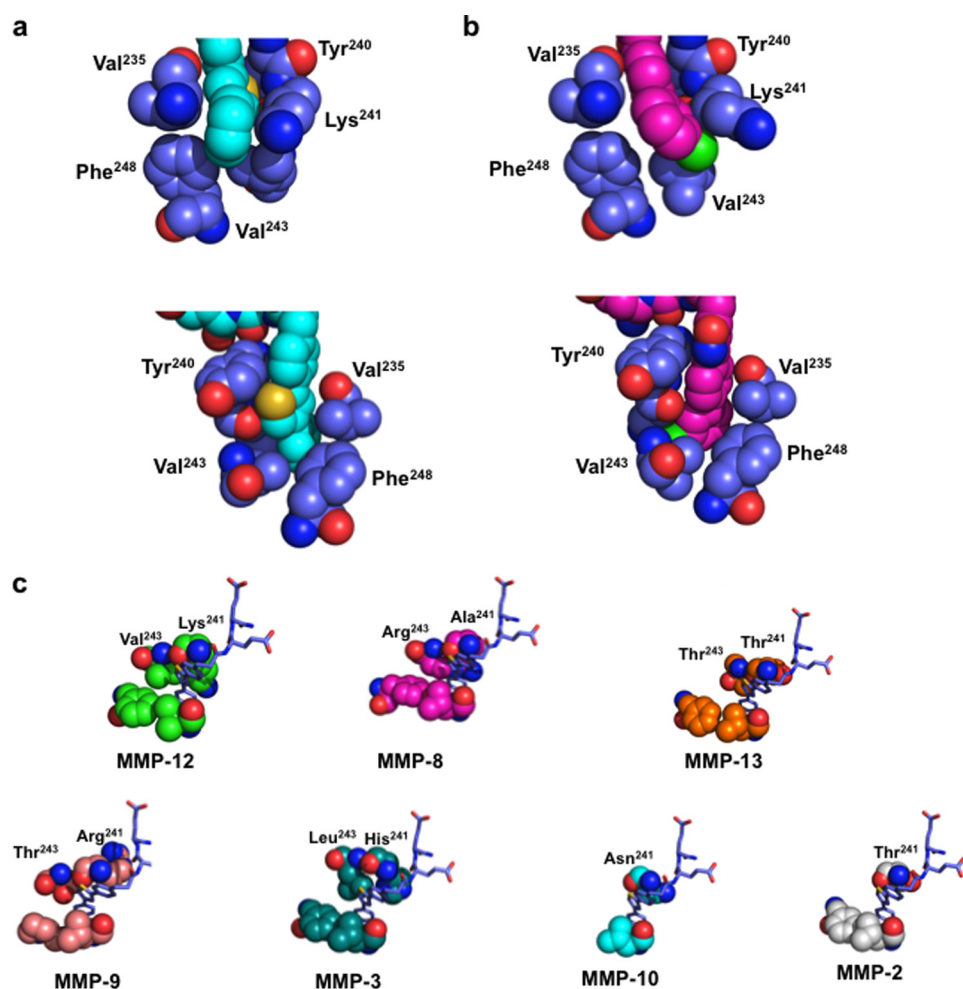
FIGURE 5. *a* and *b*, close-up views of the S_1' bottom part of MMP-12 in complex with **36** in front (*top*) and back (*bottom*) view (*a*) or in complex with **5** in front (*top panels*) and back (*bottom panels*) view (*b*). **36** is colored in *cyan*, **5** is in *magenta*, and MMP-12 residues are in *blue* (ball-stick representation). *c*, a close-up view of MMP·**36** models showing the S_1' bottom part of MMPs and the packing between the P_1' side chain of **36** and the MMP S_1' loop residues.

opposite direction, toward Phe[248] (Fig. 5*a*). Overall, the presence of a five-member ring in **36** allows better packing between the inhibitor P_1' side chain and S_1' residues (Tyr[240] and Lys[241]), compared with the P_1' side chain of **5**, so that the void volume between the inhibitor P_1' side chain and the S_1' cavity appears lower with **36**, as compared with **5** (Fig. 5, *a* and *b*). These differences may explain the higher potency of **36** toward MMP-12 and its better selectivity profile. To support this contention, we tested whether the structure adopted by **36** when bound to MMP-12 might fit in the active sites of other MMPs. Strikingly, **36** can be easily docked into other MMP active sites, without steric clash. However, these simple models reveal that the optimal close contacts observed between the distal part of the P_1' side chain of **36** and the five residues of the MMP-12 delineating the bottom part of the S_1' cavity (Val[235], Tyr[240], Lys[241], Val[243], and Phe[248]), with the exception of MMP-8, are not observed in other MMPs (Fig. 5*c*) (we selected MMPs for which the inhibitor selectivity has been improved between compound **5** and **36**). Besides differences in the S_1' loop conformation between MMPs, the above observations also arise from the variability in the nature of the residues at positions 241

and 243 in various MMPs (Fig. 5*c*). From the above considerations, the poor selectivity displayed by compound **5** may arise from the linear shape of its P_1' side chain, as compared with the bent P_1' side chain structure of **36**.

DISCUSSION

The development of most MMP inhibitors for the last 15 years has relied on the use of a strong zinc-binding group, such as hydroxamate, and by targeting the entrance of the S_1' cavity. This strategy was selected to obtain potent inhibition through tight hydroxamate/zinc ion interaction and maintaining the inhibitor in a low molecular weight range by limiting the size of the P_1' side chain. Unfortunately, although providing extremely potent MMP inhibitors, all of the compounds obtained through this strategy displayed poor selectivity toward MMPs and also targeted other unrelated zinc-metalloproteinases like NEP (14). The use of a weaker zinc-binding group (carboxylate or phosphoryl group) led to more selective inhibitors, in particular for MMP-12 (15, 48, 49). First, the present study demonstrates that pseudo-peptides with no phosphinic zinc-binding group in their structures can behave as potent MMP-12 inhibitors. Second, this study shows

that exploring the bottom part of the S_1' cavity of MMP-12 by using long and bent P_1' side chain resulted in inhibitors showing even better selectivity profile than the best selective MMP-12 reported so far (compound **4**) (15). Third, this study indicates that the inhibitor P_1' side chain accommodation into the S_1' cavity occurs without major conformational shift of the S_1' loop, in contrast to what was observed with MMP-13 selective inhibitors (16) and mixed MMP13/MMP-8 inhibitors (18). Selective MMP-13 inhibitors have been proposed to select a particular/minor conformation of MMP-13 from a conformational ensemble. Even if this concept seems to apply also to MMP-8, noncanonical S_1' loop conformation in MMPs is poorly documented; thus translation of this approach for developing selective inhibitor toward other MMPs approach remains challenging. In contrast a lot of three-dimensional structures (x-ray or NMR) of MMPs are available in which a preferred S_1' loop conformation can be potentially targeted by inhibitors probing the bottom part of the S_1' cavity for developing more selective MMP inhibitors. Although this strategy is appealing, the present study shows that subtle variations in the inhibitor structure entail profound selectivity and potency vari-

ations. Potency and selectivity are in fact a function of several linked and complex parameters. Thus, the exact positioning of the P_1' side chain inside the S_1' cavity seems to be critical. Such positioning depends on the nature of the ring (isoxazole *versus* phenyl) in the inhibitor P_1' side chain at the entrance of S_1' cavity. The shape of the P_1' side chain is also important. A long P_1' linear side chain like in **23** strongly increases the inhibitor potency but yields a poor selectivity profile. Only with a bent side chain have the best results in terms of selectivity been achieved. Compounds **5** and **36** highlight how very subtle structural differences act in synchrony to yield a different selectivity profile. The small adjustments of the residues lining the S_1' cavity in response to inhibitor binding are difficult to predict, yet such knowledge could potentiate the use of structure-based design approach to develop highly selective inhibitors. These limitations explain why the development of selective MMP inhibitors has been so disappointing in the past 20 years.

In summary, the present study reports how the systematic modification of the P_1' side chain has resulted in the identification of selective inhibitors. The absence of a zinc-binding group has facilitated the discovery process by strengthening the role played by the P_1' side chain and by removing the positional constraints associated with the zinc interaction. Considering the previous successes obtained with MMP-13, it appears extremely likely that more non-zinc-binding inhibitors of MMPs with high selectivity profile will be reported in the future. Whether such compounds will select highly or less populated S_1' loop conformations of MMPs is more difficult to foresee.

REFERENCES

1. Babine, R. E., and Bender, S. L. (1997) *Chem. Rev.* **97,** 1359–1472
2. Whittaker, M., Floyd, C. D., Brown, P., and Gearing, A. J. (1999) *Chem. Rev.* **99,** 2735–2776
3. Cuniasse, P., Devel, L., Makaritis, A., Beau, F., Georgiadis, D., Matziari, M., Yiotakis, A., and Dive, V. (2005) *Biochimie* **87,** 393–402
4. Fisher, J. F., and Mobashery, S. (2006) *Cancer Metastasis Rev.* **25,** 115–136
5. Nuti, E., Tuccinardi, T., and Rossello, A. (2007) *Curr. Pharm. Des.* **13,** 2087–2100
6. Tu, G., Xu, W., Huang, H., and Li, S. (2008) *Curr. Med. Chem.* **15,** 1388–1395
7. Yiotakis, A., and Dive, V. (2008) *Mol. Aspects Med.* **29,** 329–338
8. Fingleton, B. (2007) *Curr. Pharm. Des.* **13,** 333–346
9. Brown, S., Meroueh, S. O., Fridman, R., and Mobashery, S. (2004) *Curr. Top. Med. Chem.* **4,** 1227–1238
10. Moy, F. J., Chanda, P. K., Chen, J., Cosmi, S., Edris, W., Levin, J. I., Rush, T. S., Wilhelm, J., and Powers, R. (2002) *J. Am. Chem. Soc.* **124,** 12658–12659
11. Bertini, I., Calderone, V., Cosenza, M., Fragai, M., Lee, Y. M., Luchinat, C., Mangani, S., Terni, B., and Turano, P. (2005) *Proc. Natl. Acad. Sci. U.S.A.* **102,** 5334–5339
12. Bode, W., and Maskos, K. (2003) *Biol. Chem.* **384,** 863–872
13. Tallant, C., Marrero, A., and Gomis-Rüth, F. X. (2010) *Biochim. Biophys. Acta* **1803,** 20–28
14. Saghatelian, A., Jessani, N., Joseph, A., Humphrey, M., and Cravatt, B. F. (2004) *Proc. Natl. Acad. Sci. U.S.A.* **101,** 10000–10005
15. Devel, L., Rogakos, V., David, A., Makaritis, A., Beau, F., Cuniasse, P., Yiotakis, A., and Dive, V. (2006) *J. Biol. Chem.* **281,** 11152–11160
16. Engel, C. K., Pirard, B., Schimanski, S., Kirsch, R., Habermann, J., Klingler, O., Schlotte, V., Weithmann, K. U., and Wendt, K. U. (2005) *Chem. Biol.* **12,** 181–189
17. Johnson, A. R., Pavlovsky, A. G., Ortwine, D. F., Prior, F., Man, C. F., Bornemeier, D. A., Banotai, C. A., Mueller, W. T., McConnell, P., Yan, C., Baragi, V., Lesch, C., Roark, W. H., Wilson, M., Datta, K., Guzman, R., Han, H. K., and Dyer, R. D. (2007) *J. Biol. Chem.* **282,** 27781–27791
18. Pochetti, G., Montanari, R., Gege, C., Chevrier, C., Taveras, A. G., and Mazza, F. (2009) *J. Med. Chem.* **52,** 1040–1049
19. Morales, R., Perrier, S., Florent, J. M., Beltra, J., Dufour, S., De Mendez, I., Manceau, P., Tertre, A., Moreau, F., Compere, D., Dublanchet, A. C., and O'Gara, M. (2004) *J. Mol. Biol.* **341,** 1063–1076
20. Lagente, V., Le Quement, C., and Boichot, E. (2009) *Expert Opin. Ther. Targets* **13,** 287–295
21. Liu, M., Sun, H., Wang, X., Koike, T., Mishima, H., Ikeda, K., Watanabe, T., Ochiai, N., and Fan, J. (2004) *Arthritis Rheum.* **50,** 3112–3117
22. Halpert, I., Sires, U. I., Roby, J. D., Potter-Perigo, S., Wight, T. N., Shapiro, S. D., Welgus, H. G., Wickline, S. A., and Parks, W. C. (1996) *Proc. Natl. Acad. Sci. U.S.A.* **93,** 9748–9753
23. Curci, J. A., Liao, S., Huffman, M. D., Shapiro, S. D., and Thompson, R. W. (1998) *J. Clin. Invest.* **102,** 1900–1910
24. Rodríguez-Pla, A., Martínez-Murillo, F., Savino, P. J., Eagle, R. C., Jr., Seo, P., and Soloski, M. J. (2009) *Rheumatology* **48,** 1460–1461
25. Demedts, I. K., Morel-Montero, A., Lebecque, S., Pacheco, Y., Cataldo, D., Joos, G. F., Pauwels, R. A., and Brusselle, G. G. (2006) *Thorax* **61,** 196–201
26. Hunninghake, G. M., Cho, M. H., Tesfaigzi, Y., Soto-Quiros, M. E., Avila, L., Lasky-Su, J., Stidley, C., Melén, E., Söderhäll, C., Hallberg, J., Kull, I., Kere, J., Svartengren, M., Pershagen, G., Wickman, M., Lange, C., Demeo, D. L., Hersh, C. P., Klanderman, B. J., Raby, B. A., Sparrow, D., Shapiro, S. D., Silverman, E. K., Litonjua, A. A., Weiss, S. T., and Celedón, J. C. (2009) *N. Engl. J. Med.* **361,** 2599–2608
27. Hautamaki, R. D., Kobayashi, D. K., Senior, R. M., and Shapiro, S. D. (1997) *Science* **277,** 2002–2004
28. Morris, D. G., Huang, X., Kaminski, N., Wang, Y., Shapiro, S. D., Dolganov, G., Glick, A., and Sheppard, D. (2003) *Nature* **422,** 169–173
29. Wang, X., Inoue, S., Gu, J., Miyoshi, E., Noda, K., Li, W., Mizuno-Horikawa, Y., Nakano, M., Asahi, M., Takahashi, M., Uozumi, N., Ihara, S., Lee, S. H., Ikeda, Y., Yamaguchi, Y., Aze, Y., Tomiyama, Y., Fujii, J., Suzuki, K., Kondo, A., Shapiro, S. D., Lopez-Otin, C., Kuwaki, T., Okabe, M., Honke, K., and Taniguchi, N. (2005) *Proc. Natl. Acad. Sci. U.S.A.* **102,** 15791–15796
30. Johnson, J. L., George, S. J., Newby, A. C., and Jackson, C. L. (2005) *Proc. Natl. Acad. Sci. U.S.A.* **102,** 15575–15580
31. Coussens, L. M., Fingleton, B., and Matrisian, L. M. (2002) *Science* **295,** 2387–2392
32. Overall, C. M., and Kleifeld, O. (2006) *Br. J. Cancer* **94,** 941–946
33. López-Otín, C., Palavalli, L. H., and Samuels, Y. (2009) *Cell Cycle* **8,** 3657–3662
34. Jullien, N., Makritis, A., Georgiadis, D., Beau, F., Yiotakis, A., and Dive, V. (2010) *J. Med. Chem.* **53,** 208–220
35. Dabert-Gay, A. S., Czarny, B., Devel, L., Beau, F., Lajeunesse, E., Bregant, S., Thai, R., Yiotakis, A., and Dive, V. (2008) *J. Biol. Chem.* **283,** 31058–31067
36. Horovitz, A., and Levitzki, A. (1987) *Proc. Natl. Acad. Sci. U.S.A.* **84,** 6654–6658
37. Stura, E. A., Nemerow, G. R., and Wilson, I. A. (1992) *J. Cryst. Growth* **122,** 273–285
38. Stura, E. A., and Wilson, I. A. (1991) *J. Cryst. Growth* **110,** 270–282
39. Leslie, A. G. (2006) *Acta Crystallogr. D Biol. Crystallogr.* **62,** 48–57
40. Vagin, A. A., and Teplyakov, A. (1997) *J. Appl. Crystallogr.* **30,** 1022–1025
41. Murshudov, G. N., Vagin, A. A., and Dodson, E. J. (1997) *Acta Crystallogr. D Biol. Crystallogr.* **53,** 240–255
42. Collaborative Computational Project (1994) *Acta Crystallogr. D Biol. Crystallogr.* **50,** 760–763
43. McRee, D. E. (1999) *J. Struct. Biol.* **125,** 156–165
44. Emsley, P., Lohkamp, B., Scott, W. G., and Cowtan, K. (2010) *Acta Crystallogr. D Biol. Crystallogr.* **66,** 486–501
45. DeLano, W. L. (2002) *The PyMOL Molecular Graphics System,* DeLano Scientific, San Carlos, CA
46. Gall, A. L., Ruff, M., Kannan, R., Cuniasse, P., Yiotakis, A., Dive, V., Rio,

M. C., Basset, P., and Moras, D. (2001) *J. Mol. Biol.* **307,** 577–586

47. Tochowicz, A., Maskos, K., Huber, R., Oltenfreiter, R., Dive, V., Yiotakis, A., Zanda, M., Pourmotabbed, T., Bode, W., and Goettig, P. (2007) *J. Mol. Biol.* **371,** 989–1006

48. Li, W., Li, J., Wu, Y., Rancati, F., Vallese, S., Raveglia, L., Wu, J., Hotchandani, R., Fuller, N., Cunningham, K., Morgan, P., Fish, S., Krykbaev, R., Xu, X., Tam, S., Goldman, S. J., Abraham, W., Williams, C., Sypek, J., and Mansour, T. S. (2009) *J. Med. Chem.* **52,** 5408–5419

49. Li, W., Li, J., Wu, Y., Wu, J., Hotchandani, R., Cunningham, K., McFadyen, I., Bard, J., Morgan, P., Schlerman, F., Xu, X., Tam, S., Goldman, S. J., Williams, C., Sypek, J., and Mansour, T. S. (2009) *J. Med. Chem.* **52,** 1799–1802